Integrin $\alpha_v\beta_3$-Targeted Radioimmunotherapy of Glioblastoma Multiforme

Anand Veeravagu,[1,2] Zhaofei Liu,[4] Gang Niu,[1] Kai Chen,[1] Bing Jia,[4] Weibo Cai,[1] Cunjing Jin,[4] Andrew R. Hsu,[1] Andrew J. Connolly,[3] Victor Tse,[2] Fan Wang,[4] and Xiaoyuan Chen[1]

Abstract

Purpose: Abegrin is a monoclonal antibody to human integrin $\alpha_V\beta_3$, a cell adhesion molecule highly expressed on actively angiogenic endothelium and glioblastoma multiforme tumor cells. The purpose of this study was to evaluate the efficacy of a novel ^{90}Y-Abegrin radioimmunotherapeutic agent in murine xenograft glioblastoma models with noninvasive *in vivo* molecular imaging modalities.

Experimental Design: A s.c. U87MG human glioblastoma xenograft model was used to determine maximum tolerated dose (MTD), biodistribution, dose response, and efficacy of ^{90}Y-Abegrin. Antitumor efficacy was also characterized in an orthotopic U87MG and in a HT-29 colorectal cancer model, a low integrin-expressing carcinoma. Small-animal positron emission tomography imaging was used to correlate histologic findings of treatment efficacy.

Results: MTD and dose response analysis revealed 200 μCi per mouse as appropriate treatment dose with hepatic clearance and no organ toxicity. ^{90}Y-Abegrin – treated U87MG tumor mice showed partial regression of tumor volume, with increased tumor volumes in ^{90}Y-IgG, Abegrin, and saline groups. ^{18}F-FDG imaging revealed a reduction of cell proliferation and metabolic activity whereas ^{18}F-FLT reflected decreased DNA synthesis in the ^{90}Y-Abegrin group. Ki67 analysis showed reduced proliferative index and quantitative terminal deoxynucleotidyl transferase dUTP nick-end labeling – positive analysis revealed increased DNA fragmentation and apoptosis in ^{90}Y-Abegrin animals. CD31 and 4′,6-diamidino-2-phenylindole staining showed increased vascular fragmentation and dysmorphic vessel structure in ^{90}Y-Abegrin animals only. Orthotopic U87MG tumors treated with ^{90}Y-Abegrin displayed reduced tumor volume. HT-29 tumors showed no significant difference among the various groups.

Conclusion: Radioimmunotherapy with ^{90}Y-labeled Abegrin may prove promising in the treatment of highly vascular, invasive, and heterogeneous malignant brain tumors.

Authors' Affiliations: [1]Molecular Imaging Program at Stanford, Department of Radiology and Bio-X Program and Departments of [2]Neurosurgery and [3]Pathology, Stanford University School of Medicine, Stanford, California; and [4]Medical Isotopes Research Center, Peking University, Beijing, China

Received 3/29/08; revised 8/13/08; accepted 8/15/08.

Grant support: MedImmune, Inc. (X. Chen); National Cancer Institute R01 CA119053, R21 CA121842, R21 CA102123, P50 CA114747, and U54 CA119367 (X. Chen); Beijing Science and Technology Program Z00004105040311 and D0206001041991 (F. Wang); and National Science Foundation of China 30640067 (F. Wang).

The costs of publication of this article were defrayed in part by the payment of page charges. This article must therefore be hereby marked *advertisement* in accordance with 18 U.S.C. Section 1734 solely to indicate this fact.

Note: Supplementary data for this article are available at Clinical Cancer Research Online (http://clincancerres.aacrjournals.org/).

A. Veeravagu and Z. Liu contributed equally to this work.

Requests for reprints: Xiaoyuan Chen, Molecular Imaging Program at Stanford, Department of Radiology and Bio-X Program, Stanford University School of Medicine, 1201 Welch Road, P095, Stanford, CA 94305-5484. Phone: 650-725-0950; Fax: 650-736-7925; E-mail: shawchen@stanford.edu or Fan Wang, Medical Isotopes Research Center, Peking University, 38#, Xueyuan Road, Beijing 100083, China. E-mail: wangfan@bjmu.edu.cn.

doi:10.1158/1078-0432.CCR-08-0797

Glioblastoma multiforme is the most prevalent and malignant primary brain tumor in adults. It is a high-grade WHO class (IV) tumor that usually presents in the sixth or seventh decade of life and carries an average prognosis of 1 year (1). Standard synergistic treatment of microsurgical resection combined with postoperative external radiation and chemotherapy is not effective in significantly extending the lifespan of patients (2, 3). With a high proliferation rate, marked neovascularization, central necrosis, and extensive local invasion into normal brain parenchyma, gliomas have developed resistance to traditional radiation and chemotherapy agents (4). Current therapeutic strategies have shown poor efficacy due to lack of tumor cell specificity, poor tumor penetration, and invasive administration technique.

The discovery of tumor-specific antigens has led cancer research to focus on antibody-based therapeutics. Integrin $\alpha_V\beta_3$ is a cell adhesion molecule highly expressed on actively angiogenic endothelium and expanding glioblastoma multiforme tumoral cells (5–9), rarely expressed on nascent vascular smooth muscle endothelium (10). It is well known that

Translational Relevance

Each year over 16,000 people are diagnosed with glioblastoma multiforme in the United States. With a median survival of just under one year, maximum synergistic treatment offers little hope for palliation. Recent discoveries have identified integrin $\alpha_v\beta_3$ as a receptor uniquely expressed on the surface of malignant glioma cells. Integrin $\alpha_v\beta_3$ is capable of orchestrating the angiogenic and infiltrative behavior necessary for tumor expansion. Developing a targeted antibody capable of cellular localization will not only enable high-dose radiation delivery, but will also offer parenchymal brain sparing – a true concern for those patients with worsening neurologic deficit. In our study, we show the efficacy of ^{90}Y-Abegrin, an antibody-based radioimmunotherapeutic that localizes to the surface of cancerous cells and angiogenic vasculature, in the treatment of U87MG human glioblastoma tumors.

malignant gliomas require an immense vascular network to support tumorigenesis, parenchymal invasion, and distant metastasis (11). In this process of angiogenesis, integrin $\alpha_V\beta_3$ directs extracellular matrix adhesion to support the recruitment of endothelial progenitor cells. Additionally, malignant gliomas have been shown to express $\alpha_V\beta_3$ in great density on their cell surface (7, 12, 13). Thus, integrin $\alpha_V\beta_3$ is a reliable marker to distinguish malignant from benign cancer phenotype due to its strong correlation with tumor invasiveness, metastasis, and poor clinical outcome (14–20).

Inhibition of $\alpha_V\beta_3$ by monoclonal antibodies, cyclic RGD peptide antagonists (21), and peptidomimetics (22) has shown efficacy in halting angiogenesis (23) and tumor cell growth (24, 25). Abegrin (MEDI-522 or Vitaxin) is a humanized monoclonal antibody against human integrin $\alpha_V\beta_3$ currently in phase II clinical trials (26). It has shown high glioma-specific uptake as well as ideal pharmacokinetics and dose optimization in glioblastoma multiforme murine models (12). It is hypothesized that the "triad" of Abegrin activity results in the reduction of tumor growth, angiogenesis, and distant metastasis (27). Thus, this antibody is well suited for targeting glioblastoma multiforme cells *in vivo*.

Currently, the use of immunotherapy has been augmented with radionuclides to create radioimmunotherapeutics. Such therapeutics have been attempted and shown efficacy in a number of clinical studies. Promising results have been obtained by intracavitary and/or pretargeted radioimmunotherapeutics with ^{90}Y in high-grade gliomas (28), craniopharyngiomas (29), and non–Hodgkin's (30) and central nervous system lymphomas (31, 32). ^{90}Y is a high-energy pure β-emitter ideal for targeted radiation therapy with a physical $t_{1/2}$ of 64 hours and an effective tissue penetration of 5.3 mm (33), generating a sphere of therapeutic efficacy beyond that of bound antibody (34). Thus ^{90}Y may be uniquely suited for patients with large, bulky tumor masses with aberrant vascular networks such as malignant gliomas.

The investigation of radioimmunotherapeutics in the treatment of glioblastoma multiforme has largely focused on intracavitary or general pretargeted therapy. Although these therapeutics have shown some improvement in clinical outcome, the lack of tumor specificity increases human myelotoxicity as larger doses are required for therapeutic efficacy (35). Thus, the use of a tumor-specific antibody conjugated to a potent radionuclide may provide the level of radiotherapy and molecular inhibition necessary to treat aggressive brain tumors. The purpose of this study was to evaluate the treatment efficacy of a novel ^{90}Y-Abegrin radioimmunotherapeutic in murine xenograft glioblastoma models by use of noninvasive *in vivo* molecular imaging modalities.

Materials and Methods

DOTA conjugation and radiolabeling. ^{90}Y was obtained from Perkin-Elmer and the monoclonal antibody Abegrin was obtained from MedImmune, Inc. The synthesis of DOTA-Abegrin (1,4,7,10-tetraazadodecane-*N*,*N*′,*N*″,*N*‴-tetraacetic acid) was reported earlier (12). Briefly, ^{90}Y was added to the DOTA-Abegrin conjugates at 25 μg of DOTA-Abegrin per mCi of ^{90}Y. The reaction mixture was incubated for 1 h at 40°C with constant shaking. The ^{90}Y-DOTA-Abegrin conjugate was purified by PD-10 column using PBS as the eluent. The radioactive fractions containing ^{90}Y-DOTA-Abegrin were collected and passed through a 0.2-μm syringe filter for further *in vitro* and *in vivo* experiments. A similar procedure was used for ^{111}In-DOTA-Abegrin conjugation.

Biodistribution. Twenty nude mice were randomly divided into five groups, each of which had four animals. Each mouse was injected with 15 μCi of ^{111}In-DOTA-Abegrin via tail vein. The mice were sacrificed at 4, 24, 72, 120, and 168 h postinjection. Blood, major organs, and tissues were harvested, weighed, and measured in a γ-counter. Organ uptake was calculated as a percentage of injected dose per gram of tissue (%ID/g).

Maximum tolerated dose of ^{90}Y-Abegrin. The maximum tolerated dose (MTD) in nontumor-bearing female nude mice was determined by tail vein injection of escalating ^{90}Y doses (50, 100, 150, 200, and 300 μCi). Each dose was tested in seven mice. Body weight and health status were determined twice weekly over 35 d. Peripheral blood was collected from the tail vein twice weekly and then tested in a blood analyzer. Samples from mice within a given dose group were pooled, and diluted 1:200 in PBS for RBC counts, 1:100 in 1% (w/v) ammonium oxalate for platelet counts, or 1:20 in 3% (w/v) acetic acid for WBC and neutrophil counts. Because organ damage may not immediately present, animals were monitored for an additional 1-mo period. The MTD was set at the dose below the first dose that caused severe loss of body weight (>20%) or animal death.

U87MG glioblastoma multiforme xenograft model. The U87MG human glioblastoma multiforme cell line was obtained from American Type Culture Collection. U87MG cells were grown in DMEM and cultured in medium supplemented with 10% (v/v) fetal bovine serum (FBS) at 37°C in a humidified atmosphere with 5% CO_2.

Female athymic nude mice were supplied from Harlan at 4 to 5 wk of age. All animal procedures were done according to a protocol approved by Stanford University Institutional Animal Care and Use Committee. The U87MG brain tumor model was established by injection of 5×10^6 cells (in 50 μL PBS) into the s.c. tissue of the left shoulder. Tumor size was monitored via serial caliper measurements every 3 d. Each measurement was taken three times and averaged to provide an approximation of tumor size.

For orthotopic preparation, mice were anesthetized with i.m. ketamine, and an electric drill was used to create a 1-mm diameter burr hole 2 mm lateral and 1 mm anterior to the bregma on the right side. Following dural penetration, a 10 μL Hamilton syringe was stereotactically inserted 2.0 mm from the surface of the brain and a 5-μL suspension of 1×10^6 U87MG cells was delivered over a period of 5 min. The needle was then retracted over 5 min and the scalp was reapproximated using 5-0 vicryl sutures.

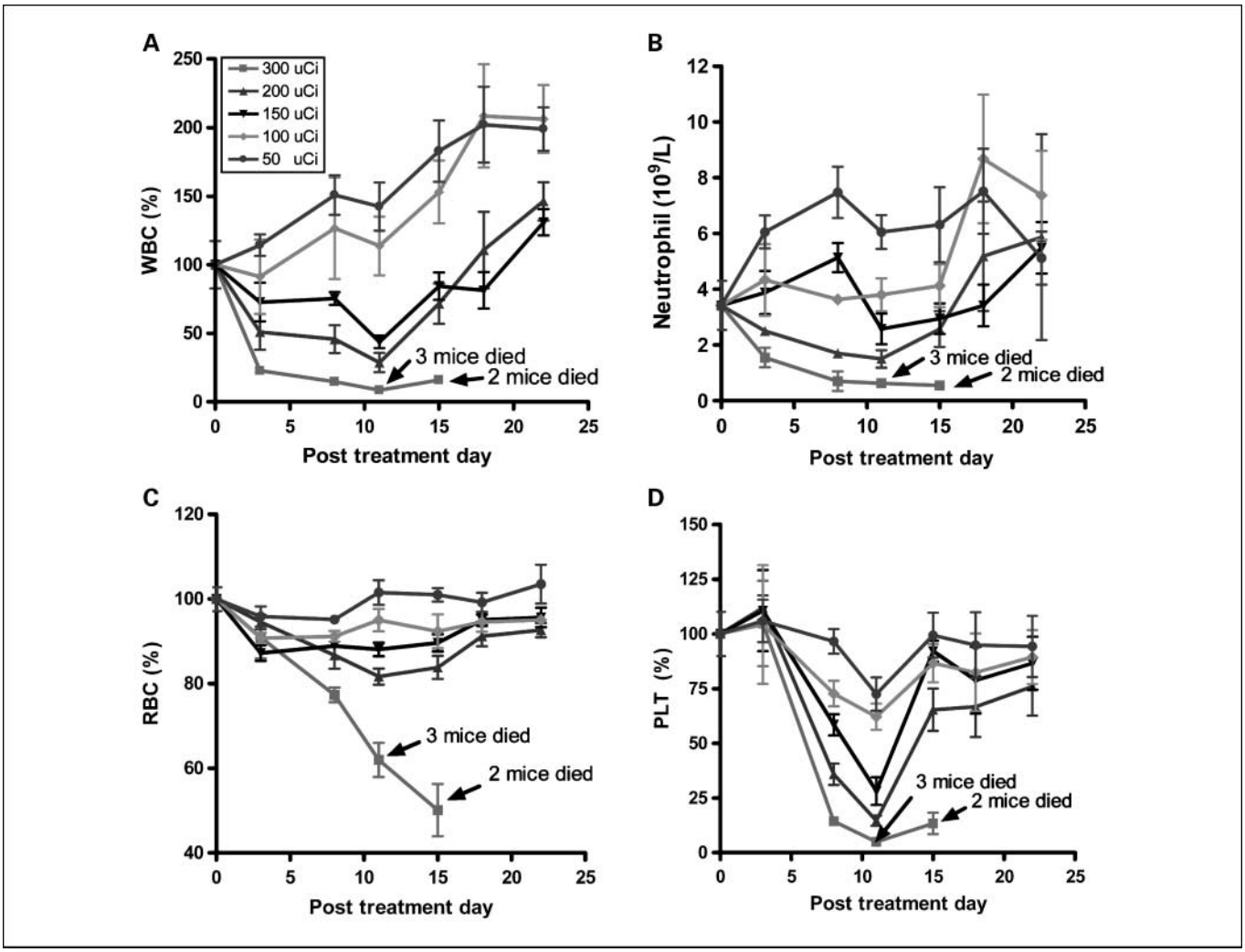

Fig. 1. A MTD study was completed using escalating ^{90}Y doses of 50, 100, 150, 200, and 300 μCi. Each dose was tested in seven female athymic nude mice. *A* to *D,* animals that received 300 μCi suffered from hematologic toxicity with a decline in WBC, neutrophil, RBC, and platelet counts, and eventual mortality. Animals that received 50, 100, 150, or 200 μCi of activity did not experience significant reductions in WBC, neutrophil, RBC, or platelet counts.

Radioimmunotherapeutic dose selection and therapy. To characterize the dose response of ^{90}Y-Abegrin, multiple escalating doses were tested in animals bearing s.c. U87MG tumors. Separated into four categories, animals received either saline or 50, 100, or 200 μCi of ^{90}Y-Abegrin. Efficacy was assessed via serial tumor size and body weight measurement.

To assess therapeutic efficacy, inoculated mice that approached a uniform tumor size of ~300 mm^3 4 wk after tumor cell inoculation were chosen for study. At this time, animals were segregated into four groups and injected with a single dose of ^{90}Y-Abegrin (n = 10), ^{90}Y-IgG (n = 5), Abegrin (n = 5), or saline (n = 9). All four groups of tumor-bearing mice were subjected to small-animal positron emission tomography (PET) imaging as well as serial tumor and body weight measurement.

HT-29 xenograft model. To evaluate the efficacy of ^{90}Y-Abegrin in low integrin-expressing cancers, a 50-μL suspension of 5 × 10^6 HT-29 cells, human colon cancer, was injected s.c. into the upper right flanks of female athymic nude mice. Animals with visible tumor growth were again separated into three groups and received either 200 μCi of ^{90}Y-Abegrin, 200 μCi of ^{90}Y-IgG, or saline. These animals underwent serial tumor and body weight measurement.

Small-animal PET imaging. PET imaging of tumor-bearing mice was done on a microPET R4 rodent model scanner as previously described (34). Mice were injected with ^{18}F-FLT (^{90}Y-Abegrin: 7 mice; ^{90}Y-IgG: 4 mice; Abegrin: 5 mice; control: 5 mice) or ^{18}F-FDG (^{90}Y-Abegrin: 7 mice; ^{90}Y-IgG: 4 mice; Abegrin: 5 mice; control: 4 mice) via the tail vein, anesthetized with 2% isoflurane and placed near the center of the field of view where the highest image resolution and sensitivity was available. Assuming a tissue density of 1 g/mL, the counts per milliliter per minute were converted to counts per gram per minute, and then divided by the injected dose (ID) to obtain an imaging region of interest – derived percentage ID per gram of tissue (%ID/g) as previously described (36 – 38).

Histopathologic processing. Visualization of collagen fibers and cellular architecture was achieved by use of our trichrome staining protocol. Briefly, sections were incubated in Weigert's iron hematoxylin working solution, incubated with Biebrich scarlet-acid fuchsin solution, and differentiated in phosphomolybdic-phosphotungstic acid solution until collagen was not red. Sections were transferred to aniline blue, differentiated in 1% acetic acid, quickly dehydrated through 95% ethyl alcohol, and mounted with resinous medium.

For Ki67 staining, an antigen retrieval kit from Abcam was used according to the manufacturer's specifications. Endogenous peroxidase was blocked with 3% hydrogen peroxide in PBS and incubated with a protein-blocking solution containing PBS (pH 7.5). Samples were incubated with a 1:100 dilution of Ki67, incubated in diaminobenzidine, mounted on glass slides, and coverslipped.

For visualization of endothelial cells, CD31 staining was chosen. Frozen tissue sections (7 μm) were fixed with cold acetone, incubated with a protein-blocking solution, and incubated with a 1:100 dilution of rat monoclonal anti-CD31 antibody (BD Pharmingen) and 1:200 Cy5-conjugated donkey antimouse secondary antibody. Samples were mounted with 4′,6-diamidino-2-phenylindole (DAPI) for staining of cell nuclei.

Immunofluorescent terminal deoxynucleotidyltransferase-mediated biotin-dUTP nick-end labeling (TUNEL) analysis was done by use of a commercially available kit (Roche Applied Science). According to the manufacturer's specifications, samples were fixed with 10% formalin (methanol free) and permeabilized by incubation with 0.2% polyethylene glycol. Reaction buffer was added for incubation in a humidified chamber. The reaction was terminated with 30 mmol/L NaCl and 3 mmol/L sodium citrate (pH 7.2), followed by removal of unincorporated fluorescein-dUTP and staining of nuclei with DAPI.

Fluorescence images were acquired with an Axiovert 200M fluorescence microscope equipped with a DAPI (excitation, HQ 365 nm; emission, HQ 397 nm), Texas Red (excitation, HQ 535 nm; emission, HQ 610 nm), and Cy5.5 (excitation, HQ 665/45 nm; emission, HQ 725/50 nm) filter set. Images were obtained with a thermoelectrically cooled charge-coupled device and analyzed with MetaMorph software.

Volumetric histology was done on animals inoculated with orthotopic U87MG tumors. Animals were sacrificed on posttreatment day 14, and brain tissue was harvested after systemic perfusion with 20 mL cold saline followed by 20 mL of 10% formalin. A combination of sharp and blunt dissection was used to differentiate tumors from benign parenchymal tissue. Isolated tumors underwent volumetric measurement.

Statistical analysis. Quantitative data were expressed as mean ± SD. Statistical analysis was done using a 1-way ANOVA for multiple groups and an unpaired Student's *t* test. *P* values <0.05 were considered statistically significant (GraphPad Prism).

Results

Dose escalation and toxicity evaluation. Nontumor-bearing mice were separated into five groups, each of which underwent a single injection of ^{90}Y (50, 100, 150, 200, and 300 μCi).

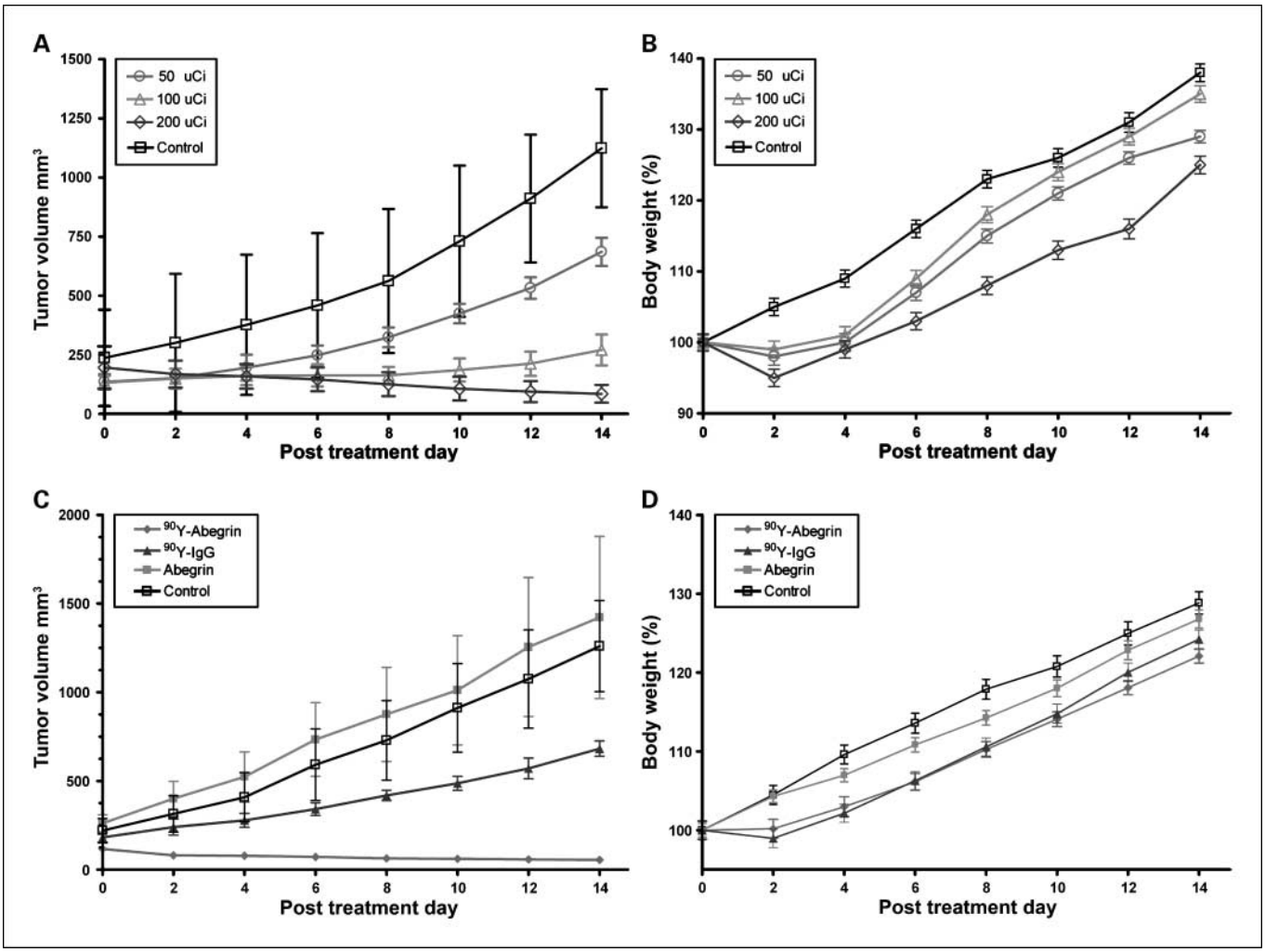

Fig. 2. ^{90}Y-Abegrin dose response and inhibition of human glioblastoma multiforme tumor growth *in vivo*. *A* and *B,* female athymic nude mice bearing U87MG tumors were injected with a one-time dose of saline, 50 μCi, 100 μCi, or 200 μCi of ^{90}Y-Abegrin. Final fractional tumor volumes revealed statistically significant differences among the treatment groups with little difference in body weight. *C,* female athymic nude mice bearing U87MG tumors were also injected with a one-time dose of 200 μCi of ^{90}Y-Abegrin, ^{90}Y-IgG, Abegrin, or saline. The growth inhibition of experimental groups was monitored via serial caliper measurements. ^{90}Y-Abegrin treatment animals maintained a statistically significant reduction in tumor size beginning on posttreatment day 2 and eventually showed partial tumor regression whereas all other groups showed increased final fractional tumor volumes. *D,* animal body weight continued to increase posttreatment, with no statistically significant difference between ^{90}Y-Abegrin and other animals.

Animal body weight, WBC, neutrophil, RBC, HCG, and platelet counts were analyzed after radioisotope injection. Only the 300 μCi group experienced animal death on postinjection days 10 and 15. The remaining 200, 150, 100, and 50 μCi groups had a final weight increase on postinjection day 32 to 136.2 ± 8.3%, 135.7 ± 11.7%, 145.5 ± 10.1%, and 146.0 ± 12.0% of the original body weight on day 0, respectively (Supplementary Fig. S1A). The WBC count of each dosage group was tracked over 22 days (Fig. 1A). Animals in the 300 μCi group experienced a reduction of WBC to 15.9 ± 1.3% of their original value. All other groups maintained a varying degree of increasing WBC with the 200 μCi group to 146.3 ± 36.9%, the 150 μCi group to 131 ± 27.08%, the 100 μCi group to 206.3 ± 60.6%, and the 50 μCi group to 199.1 ± 38.8%. Final absolute neutrophil counts were 0.55 ± 0.071 in the 300 μCi (day 15), 5.87 ± 6.40 in the 200 μCi, 5.49 ± 2.44 in the 150 μCi, 7.38 ± 3.19 in the 100 μCi, and 5.12 ± 2.33 in the 50 μCi group (Fig. 1B). RBC counts of the 300 μCi group were reduced to 50.1 ± 12.4%, the 200 μCi group to 92.7 ± 4.5%, the 150 μCi group to 95.6 ± 6.5%, the 100 μCi group to 95.1 ± 2.3%, and the 50 μCi group to 103.6 ± 11.2% of their original value (Fig. 1C). Platelet counts were also followed and revealed reduced counts with increasing dosage. Final counts 22 days postinjection were 13.6 ± 9.7% for the 300 μCi, 76.0 ± 35.2% for the 200 μCi, 86.6 ± 34.3% for the 150 μCi, 89.4 ± 24.6% for the 100 μCi, and 94.3 ± 37.1% for the 50 μCi group (Fig. 1D). HGC also showed a similar trend with the 300, 200, 150, 100, and 50 μCi groups having values of 51.9 ± 12.9%, 97.4 ± 6.8%, 100.2 ± 8.3%, 96.7 ± 2.4%, and 105.7 ± 10.1%, respectively (Supplementary Fig. S1B).

Animals in the 150, 200, and 300 μCi groups experienced a reduction in WBC, neutrophil, and platelet counts on day 11, which may represent an initial burden on the bone marrow system. Counts continued to increase, however, with some returning to physiologic levels. Overall, animals that received 300 μCi experienced a reduction in all hematologic counts and had a higher rate of mortality.

Biodistribution of ^{111}In-Abegrin. Animals injected with ^{111}In-Abegrin showed rapid and high uptake in liver and spleen to 24.81 ± 1.31 and 14.06 ± 1.79 %ID/g at 4 hours postinjection with slow washout to 7.99 ± 1.26 and 6.30 ± 3.0 %ID/g at 168 hours postinjection, respectively (Supplementary Fig. S2). ^{111}In-Abegrin was cleared rapidly from the blood 31.31 ± 7.16, 13.69 ± 1.08, 4.60 ± 2.61, 1.36 ± 0.70, and 1.17 ± 1.74 %ID/g at 4, 24, 72, 120, and 168 hours, respectively. The route of excretion was hepatic and splenic,

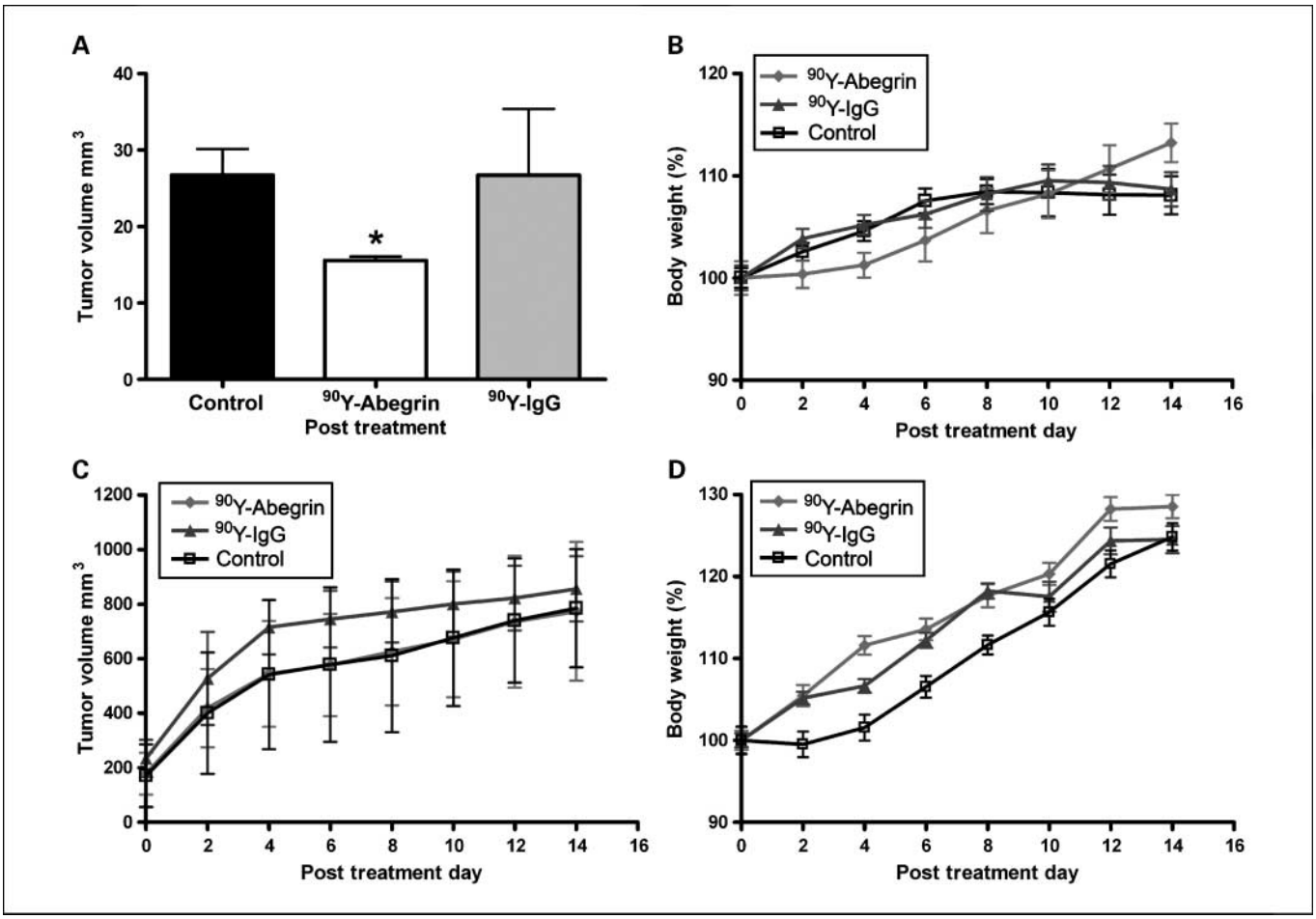

Fig. 3. Orthotopic efficacy and integrin specificity. *A,* animals bearing orthotopic tumors were divided into three experimental groups and received either 100 μCi of ^{90}Y-Abegrin, 100 μCi of ^{90}Y-IgG, or saline injection. Volumetric histology was used to assess therapeutic effect. *B,* animal body weight was monitored. *C,* low integrin expressing HT-29 cells were s.c. injected into the flanks of female athymic nude mice and animals received either 100 μCi of ^{90}Y-Abegrin, 100 μCi of ^{90}Y-IgG, or saline injection. Serial caliper measurements were used to assess tumor regression. *D,* animal body weight was also tracked over treatment time period.

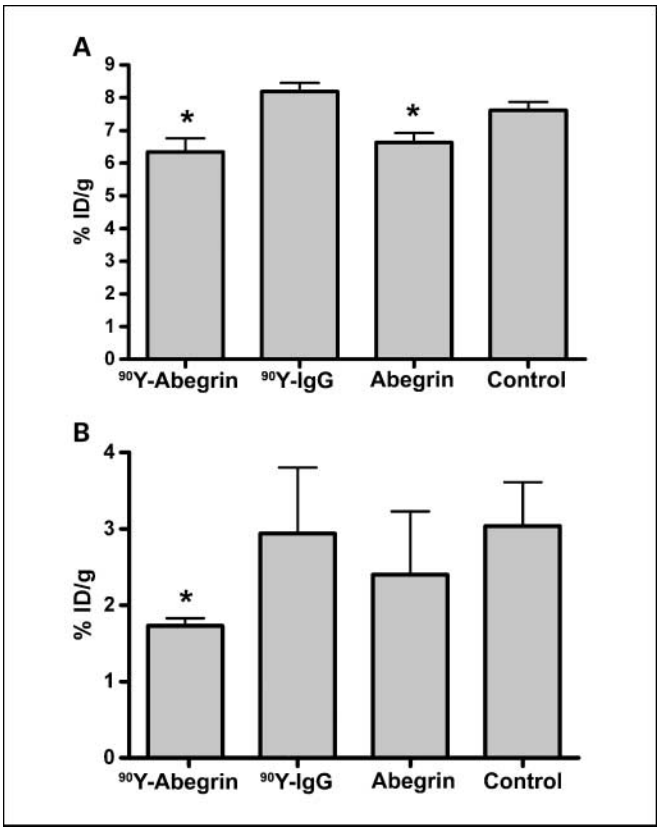

Fig. 4. Small-animal PET scans of female athymic nude mice bearing U87MG tumors treated with ^{90}Y-Abegrin, ^{90}Y-IgG, Abegrin, or saline. *A*, ^{18}F-FDG radiotracer imaging revealed a statistically significant reduction in both ^{90}Y-Abegrin and Abegrin signal intensity, suggesting reduced metabolic activity. *B*, ^{18}F-FLT radiotracer imaging showed reduced tumor accumulation value in ^{90}Y-Abegrin group, reflecting reduced DNA synthesis.

as evidenced by reduced renal concentrations of 8.39 ± 1.28 and 1.14 ± 0.49 %ID/g at 4 and 168 hours, respectively, consistent with our previous finding of ^{64}Cu-Abegrin (12). Nontarget organs such as gastrointestinal, heart, lungs, muscle, and bone all maintained low levels of ^{111}In-Abegrin.

Dose response efficacy. To evaluate the efficacy of tumor regression with respect to the dose of radioimmunotherapeutics, animals underwent treatment with a single injection of saline or 50, 100, or 200 μCi of ^{90}Y-Abegrin. Initially, all groups began with an average tumor size between 130 and 240 mm^3 (Fig. 2A). A statistically significant difference was observed on posttreatment day 14 among the four groups ($P < 0.05$). Specifically, final fractional tumor volumes ($V_{final}/V_{initial}$) of 4.74 in the control, 5.03 in the 50 μCi group, 2.04 in the 100 μCi group, and 0.43 in the 200 μCi group were obtained. Animal weight was also tracked over the experimental groups; no statistically significant difference was revealed on post treatment day 14 (Fig. 2B).

Anti–glioblastoma multiforme efficacy. The growth inhibition of experimental groups was monitored via serial caliper measurements. Initially, all groups began with an average tumor size between 150 and 300 mm^3 (Fig. 2C). ^{90}Y-Abegrin treatment animals maintained a statistically significant reduction in tumor size beginning on posttreatment day 2 and eventually showed partial tumor regression with a final fractional tumor volume ($V_{final}/V_{initial}$) of 0.69. All other groups showed increased final fractional tumor volumes of 3.76 for ^{90}Y-IgG, 5.43 for Abegrin, and 5.72 for control animals ($P < 0.0001$). Further, animal body weight continued to increase posttreatment, with no statistically significant difference between ^{90}Y-Abegrin and other animals (Fig. 2D).

Animals bearing orthotopic tumors were divided into three experimental groups and received either 100 μCi of ^{90}Y-Abegrin, 100 μCi of ^{90}Y-IgG, or saline injection. Volumetric histology revealed a final tumor volume of 15.56 ±.49, 26.72 ± 8.68, and 26.94 ± 3.46 mm^3 in the three groups, respectively (Fig. 3A). Only a reduction in the ^{90}Y-Abegrin group was of statistical significance ($P < 0.005$). Animal body weight did not reveal significant differences (Fig. 3B).

Integrin $\alpha_V\beta_3$ specificity. To assess the specificity of integrin targeting in producing tumor reduction, a low integrin-expressing cancer cell line was chosen. HT29 cells, a colorectal carcinoma, injected s.c. were randomized into three groups. Animals received 100 μCi of ^{90}Y-Abegrin, 100 μCi of ^{90}Y-IgG, or saline injection. They obtained final fractional tumor volumes of 4.35, 3.67, 4.59, respectively (Fig. 3C). Both final tumor sizes and animal body weight did not significantly differ among the three groups ($P > 0.05$; Fig. 3D).

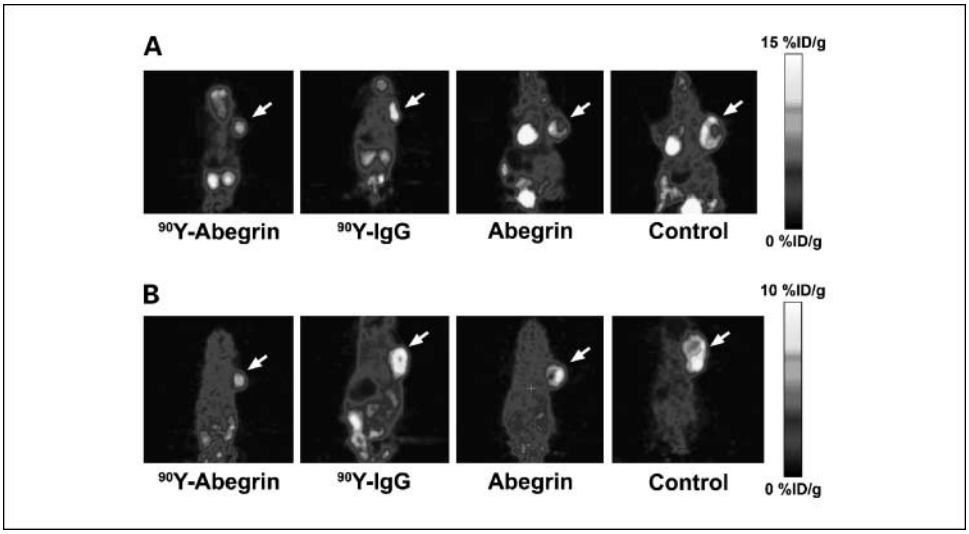

Fig. 5. PET Images. Corresponding sagittal PET images displaying the visible differences in FDG (*A*) and FLT (*B*) imaging.

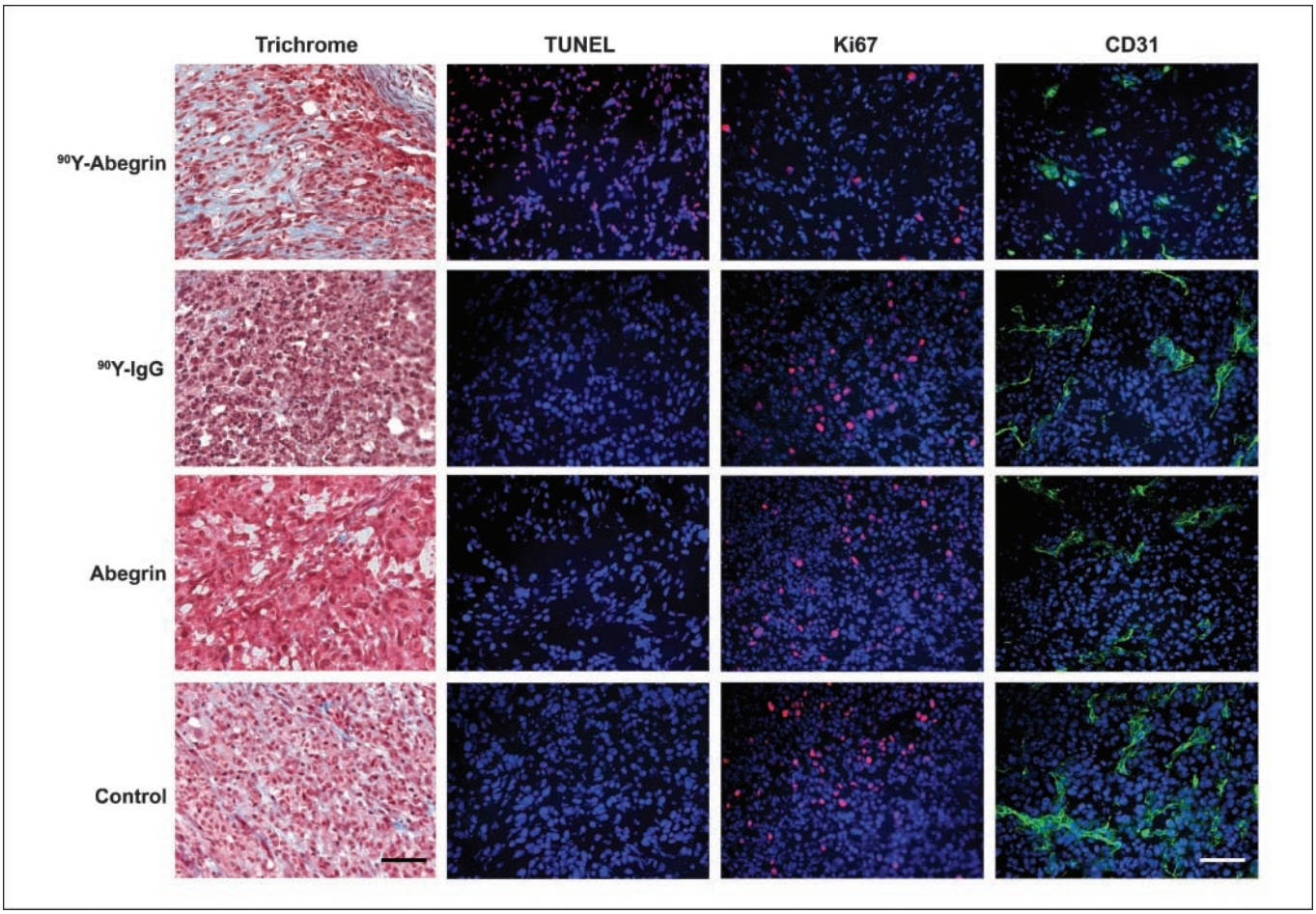

Fig. 6. *Ex vivo* illustration of ^{90}Y-Abegrin antitumor efficacy. Female athymic nude mice bearing U87MG tumors subjected to either ^{90}Y-Abegrin, ^{90}Y-IgG, Abegrin, or saline underwent trichrome, TUNEL, Ki67, and CD31/DAPI staining. Scale bar, 100 μm.

PET imaging. Small-animal PET imaging was used to characterize the *in vivo* treatment efficacy. ^{18}F-FDG and ^{18}F-FLT radiotracers were used to quantify tumor cell metabolic activity and DNA synthesis, respectively. ^{18}F-FDG imaging revealed a small but statistically significant reduction in both ^{90}Y-Abegrin (6.34 ± 0.42 %ID/g) and Abegrin (6.63 ± 0.29 %ID/g) signal intensity when compared with saline control (7.62 ± 0.25 %ID/g; $P < 0.001$), indicating a reduction in cell proliferation and metabolic activity (Fig. 4A). ^{18}F-FLT imaging showed tumor accumulation values 2 hours post injection of 1.73 ± 0.1 %ID/g in ^{90}Y-Abegrin, 2.94 ± 1.5 %ID/g in ^{90}Y-IgG, 2.39 ± 0.28 %ID/g in Abegrin, and 3.04 ± 1.28 %ID/g in control, reflecting reduced DNA synthesis in the ^{90}Y-Abegrin group ($P < 0.001$; Fig. 4B). Representative sagittal images are shown in Fig. 5A and B.

Ex vivo *validation of ^{90}Y-Abegrin radioimmunotherapeutics.* Frozen sections were recovered for trichrome, Ki67, CD31/DAPI, and TUNEL staining (Fig. 6). In ^{90}Y-Abegrin treatment mice, trichrome analysis revealed increased extracellular matrix deposition, tumor cell necrosis with diffuse interstitial fibrosis, fibrin stranding, and a significant presence of degenerated peripheral vasculature, suggesting tumor regression. ^{90}Y-IgG treatment mice showed piecemeal necrosis and hypereosinophilia with significantly greater neutrophil infiltration than ^{90}Y-Abegrin. Both control and Abegrin groups showed mitotically active tumor cells, abnormal and irregular microvasculature, and marginating neutrophils. The vasculature surrounding the necrotic center displayed cavernous capillaries, likely generated to support tumor expansion.

Ki67 analysis showed reduced proliferative index in the treated mice (4.79 ± 0.42%), whereas the ^{90}Y-IgG, Abegrin, and control animals had significantly higher proliferative indices of 8.9 ± 1.2%, 13.4 ± 2.1%, and 16.5 ± 0.7% ($P < 0.005$), respectively.

Quantitative TUNEL-positive cell analysis revealed increased DNA fragmentation and apoptosis in ^{90}Y-Abegrin animals when compared with all other groups. The ^{90}Y-Abegrin animals had significantly higher percentage of TUNEL-positive cells than the ^{90}Y-IgG, Abegrin, and control groups ($P < 0.0001$). CD31 and DAPI staining showed increased vascular fragmentation, dysmorphic vessel structure, and reduced endothelial presence in ^{90}Y-Abegrin animals.

Discussion

This study shows that ^{90}Y-Abegrin, a humanized monoclonal antibody against human integrin $\alpha_V\beta_3$, exhibits high integrin $\alpha_V\beta_3$ specificity and therapeutic efficacy against human glioblastoma multiforme tumors. The discovery and clinical translation of a nontoxic, targeted, noninvasive radioimmunotherapeutic

for glioblastoma multiforme offers new hope for survival and improved quality of life to patients diagnosed with malignant brain tumors.

We have previously shown the optimization of the DOTA/Abegrin ratio for *in vivo* targeting and maximized tumor uptake (12). The conjugate with the most DOTA residues per Abegrin was chosen for conjugation as it increases the specific activity of the tracer as well as the absolute uptake within the tumor. Further, DOTA conjugation of Abegrin does not deteriorate the receptor affinity of the antibody (data not shown). Thus DOTA-Abegrin compounds are ideal for radionuclide conjugation and targeting of $\alpha_V\beta_3$.

Currently, there are no clinical or preclinical trials that evaluate the MTD and associated toxicities of ^{90}Y-Abegrin. Human studies that evaluated the toxicity of ^{90}Y conjugated to other targeting probes found neutropenia and thrombocytopenia to be common side effects (39–41). Our goal was to develop a one-time dose therapeutic capable of exerting long-term radiation to isolated areas of malignancy. Of the doses chosen for evaluation, 300 μCi resulted in profound animal mortality within 10 to 15 days of administration. Doses of 200 μCi and less did not produce animal death or any statistical difference in body weight, WBC, neutrophil, RBC, platelet, and HGC counts during the observation period (Fig. 1). Subphysiologic levels of WBC, neutrophils, and platelets were shown on posttreatment day 11 in many of the experimental groups. Whereas bone marrow toxicity is a definite concern, the subsequent increase of these values may indicate an acute toxic burden that gradually improves without permanent localization of radioactivity. Furthermore, dose response analysis showed maximal antitumor efficacy in the 200 μCi group without animal mortality (Fig. 2A and B). Given these results, 200 μCi was chosen as our target radionuclide dose.

The advantage of highly selective tumor localization is low radiation burden to nontarget tissues. Vital organ systems such as the hepatic, renal, hematologic, intestinal, bone marrow, and disease-free brain are spared of devastating side effects and toxicity, as seen with ^{90}Y-Abegrin. Previously, to achieve therapeutic levels of radiation within tumor tissue, large, potentially toxic, doses of systemic therapy had to be administered (42). To determine the biodistribution of ^{90}Y-Abegrin, we chose ^{111}In-Abgerin as an imaging surrogate. The biodistribution of ^{111}In and ^{90}Y-labeled antibodies, proteins, and peptides has been shown to be biologically equivalent with respect to their uptake in tumors and other major organs (43). Consistent with previous reports of Abegrin biodistribution, our therapeutic shows little accumulation in areas of critical importance, such as bone marrow and circulating blood (12). The highest levels of antibody were found in liver and spleen, suggesting a spleno-hepatic clearance mechanism likely due to the high molecular weight of the antibody (~150 kDa; Supplementary Fig. S2; ref. 12). Nontarget organs such as the kidney and the intestine maintained low antibody concentration, reducing the likelihood of their function in clearance. Further, serum $t_{1/2}$ of ^{90}Y-Abegrin was found to be 12 to 24 hours, shorter than the $t_{1/2}$ of Abegrin in humans.

Monoclonal antibody–based therapeutics offer a number of advantages that make them more amenable to clinical translation. Specifically, radionuclide conjugated antibodies exert their antitumor effect by localizing continuous decaying low-dose-rate irradiation to the area of malignancy. Because ^{90}Y β-particle emission can penetrate up to 5 mm of tissue, this therapeutic can destroy antigen-negative tumor cells that have no specific antibody localized to their cell surface (44). This crossfire effect proves tremendously valuable in the case of glioblastoma multiforme, a heterogeneous tumor that lacks organized vascular structure. Ultimately this may translate into lower dosage requirement, reduced toxicity, noninvasive administration and thus a much better quality of life.

With the above parameters in mind, ^{90}Y-Abegrin is ideally suited for anti–glioblastoma multiforme therapy. In our study, partial tumor regression was successfully achieved by a one-time dose of 200 μCi of ^{90}Y-Abegrin. Animals in the treatment group reached a final fractional tumor volume of 0.68 with stable weight gain and no increase in toxicity or mortality (Fig. 2C and D). Those animals in the ^{90}Y-IgG and Abegrin groups had a much larger final fractional tumor volume, with no significant difference from control animals. The antiangiogenic effects of ^{90}Y-Abegrin resulted in reduced CD31$^+$ vascular endothelial cells, whereas control animals maintained increased vascular caliber and density (Fig. 6). Similarly, trichrome analysis showed a significant presence of degenerated peripheral vasculature in treated animals, suggesting tumor regression and vascular collapse. Control and Abegrin groups, however, showed mitotically active tumor cells and cavernous capillaries depicting active angiogenesis.

To evaluate the necessity of integrin targeting in inducing tumor regression, HT-29, low integrin-expressing, human colon adenocarinoma tumors were also examined. Previous studies have shown low cross reactivity of Abegrin with murine $\alpha_v\beta_3$,suggesting a low probability of antibody localization to xenograft integrin-negative tumors (12). It was our suspicion that due to the low expression of integrin by HT-29, binding of Abegrin is very unlikely and thus therapeutic efficacy would not be evident. Final fractional tumor volumes revealed no significant difference among the three groups, suggesting lack of therapeutic efficacy (Fig. 3C and D).

Noninvasive ^{18}F-FDG and ^{18}F-FLT small-animal PET imaging was used to quantify the rate of cell apoptosis and proliferation. Treatment animals showed a statistically significant reduction in ^{18}F-FLT signal intensity, indicating decreased cellular proliferation and tumor expansion (Figs. 4A and 5A). Consistent with these findings, *ex vivo* Ki67 histology revealed a reduced proliferative index in treatment animals, indicating low levels of active mitogenesis (Fig. 6). As seen in our study, the strong correlation of ^{18}F-FLT and Ki67 findings have been previously reported as prognostic indicators for malignant brain tumors (45).

In vivo molecular imaging techniques provide real-time functional information of tumor behavior. The ability to noninvasively characterize tumor integrin expression, vascular permeability, and proliferation will allow for more accurate patient selection, monitoring, and therapeutic intervention. In the case of glioblastoma multiforme, ^{18}F-FDG has shown poor specificity in characterizing size, functional activity, and heterogeneity of primary and recurrent brain tumors due to the high basal glucose metabolic rate of normal brain tissue. Specifically, ^{18}F-FDG uptake of low-grade tumors is similar to that of normal white matter, and high-grade tumor uptake may approximate normal gray matter, decreasing the sensitivity of tumor detection (45). FLT-based small-animal PET imaging is more sensitive for intracranial malignancies due to its inability

to cross the blood-brain barrier (BBB) and thus reduce nonspecific uptake (46). However, this functionally results in increased FLT signal intensity only in areas of BBB breakdown, reducing our capacity to discern among other possible malignant or infectious processes (47).

To more closely simulate clinical conditions, animals underwent orthotopic implantation of U87MG tumor cells. Although this remains a xenograft model, our intention was to more closely replicate the neurologic deficits produced by an enlarging intracranial mass and evaluate the efficacy of ^{90}Y-Abegrin in penetrating the BBB. In the context of malignant brain neoplasms, it is often assumed that BBB breakdown has occurred, but therapeutic penetration is still of chief concern. If considered as adjuvant therapy to supplement surgical resection or radiosurgical treatment, physical trauma induced by these modalities will often violate the integrity of the BBB. Our analysis revealed statistically significant tumor reduction in those animals receiving ^{90}Y-Abegrin, suggesting either breakdown or the ability to permeate through the BBB (Fig. 3A and B).

The mechanism by which ^{90}Y-Abegrin exerts its therapeutic effect is likely multifactorial. The radioactive decay of ^{90}Y-Abegrin is one of the most powerful β-emitting radioimmunotherapeutics tested, at 939 keV per disintegration. This allows for deep tumor penetration and effective radiation-induced cytotoxicity to cancerous cells while sparing nontarget organs and parenchymal brain tissue (48). In contrast to β-particles, α-particle emission has a shorter path length, is more focused, less diffuse, and lacks deep tumor penetration (49). In the case of malignancies that develop an organized vascular network, α-emission may prove less toxic to normal tissue, but it is likely that α-particles would not penetrate the devascularized and bulky areas of glioblastoma multiformes. Similarly, γ-ray photon emission of ^{177}Lu and ^{111}In, although useful for imaging, deposit little energy within surrounding tissue, thereby exerting futile cytotoxic effect (50). Clinical studies have shown safety and some efficacy in the use of ^{90}Y as adjuvant therapy for malignant brain tumors (51–53), but further phase II clinical trials are needed to establish true therapeutic potential. In preclinical studies ^{90}Y-labeled antibodies induced glioma regression and prolonged survival, but few antibodies possess both tumor and vascular targeting function (54).

Currently in phase II clinical trials, Abegrin is advantageous in that in addition to targeting endothelial cells of highly vascular tumors it also targets $\alpha_V\beta_3$ expressed on nascent glioma cells, further localizing therapy. To date, no preclinical or clinical study has examined the role of Abegrin therapy in high-grade gliomas, but a number of groups have investigated RGD peptide antagonists against $\alpha_V\beta_3$. Preclinical *in vivo* trials with IS20I (55) and cyclic RGD peptides (13, 56) have all shown some degree of glioma growth inhibition, but assessment of toxicity, recurrence, and functional mechanism have not been reported. In our study, Abegrin treatment alone did not induce tumor regression, apoptosis, or vascular injury. One possible reason may be the "dose-limited" antitumor activity whereby high-dose Abegrin therapy does not induce the same tumor regression observed at low doses (27). Thus, the majority of cytotoxicity seen with ^{90}Y-Abegrin may be attributed to radiation-induced damage rather than $\alpha_V\beta_3$ signaling inhibition. RGD peptide antagonists have shown efficacy in increasing radiation sensitivity of glioma cells by suppressing integrin expression. It is hypothesized that radiation-induced cell damage initiates up-regulation of $\alpha_V\beta_3$ expression and Akt signaling as a defense mechanism to stabilize injured vasculature, promoting radiation resistance (5). Thus, ^{90}Y-Abegrin likely acts synergistically to thwart host repair mechanisms and induce both vascular and tumor cell death.

The xenograft model examined in the present study may not be a true approximation of clinical utility. Anatomically, s.c. tumor implantation circumvents the restrictions of a BBB, which may account for the high uptake of ^{90}Y-Abegrin observed within tumor tissue, making the value of FLT versus FDG imaging difficult to derive. Similarly, the degree of radiation experienced by parenchymal brain tissue and resulting neurologic deficits due to mass effect and radiation injury could not be assessed; further survival-based orthotopic studies would help clarify these concerns.

To fully translate human dosimetry of ^{90}Y-Abegrin, large animal studies with sequential neurologic evaluation would prove valuable. Abegrin has been shown to cross-react with both hamster and primate $\alpha_V\beta_3$, making these animal models crucial for clinical translation. Although the current study did evaluate MTD, further examination of minimum dose necessary would reduce toxicity and aid in determining human dosimetry. Activity fractionation combined with multiple-dose regimens may reduce nontarget organ radiation and avoid systemic side effects. Current treatment for glioblastoma multiforme involves gross tumor resection, adjuvant stereotactic radiosurgery, chemotherapy, and aggressive imaging surveillance. Major considerations with such a strategy include high tumor recurrence rate, systemic chemotoxicity, radiation-induced parenchymal brain damage, and refractory treatment resistance (2). ^{90}Y-Abegrin would likely play a role as synergistic neoadjuvant therapy reducing tumor size, parenchymal invasion, and vascularity before tumor resection. This may influence the safety of surgical resection by reducing the risk of hemorrhage, maintaining clear tumor margins, and possibly reducing postoperative neurologic deficit. With the ability to noninvasively image tumors for integrin expression, we may potentially screen patients for therapeutic candidacy, increasing the likelihood of efficacy and also providing prognostic value.

Disclosure of Potential Conflicts of Interest

No potential conflicts of interest were disclosed.

Acknowledgments

We thank Drs. Fredrick T. Chin, Murugesan Subbarayan, and David W. Dick for the production of ^{18}F-FDG and ^{18}F-FLT, and Beth Hoyte for her contribution to preparation of the figures.

References

1. Stark AM, Nabavi A, Mehdorn HM, Blomer U. Glioblastoma multiforme-report of 267 cases treated at a single institution. Surg Neurol 2005;63:162–9.
2. Hou LC, Veeravagu A, Hsu AR, Tse VC. Recurrent glioblastoma multiforme: a review of natural history and management options. Neurosurg Focus 2006;20:E5.
3. Santarelli JG, Sarkissian V, Hou LC, Veeravagu A, Tse V. Molecular events of brain metastasis. Neurosurg Focus 2007;22:E1.

4. Folkman J. Angiogenesis: an organizing principle for drug discovery? Nat Rev Drug Discov 2007;6: 273–86.

5. Abdollahi A, Griggs DW, Zieher H, et al. Inhibition of $\alpha_v\beta_3$ integrin survival signaling enhances antiangiogenic and antitumor effects of radiotherapy. Clin Cancer Res 2005;11:6270–9.

6. Hsu AR, Veeravagu A, Cai W, Hou LC, Tse V, Chen X. Integrin $\alpha_v\beta_3$ antagonists for anti-angiogenic cancer treatment. Recent Patents Anticancer Drug Discov 2007;2:143–58.

7. Lim M, Guccione S, Haddix T, et al. ávâ3 Integrin in central nervous system tumors. Hum Pathol 2005; 36:665–9.

8. Mahabeleshwar GH, Feng W, Reddy K, Plow EF, Byzova TV. Mechanisms of integrin-vascular endothelial growth factor receptor cross-activation in angiogenesis. Circ Res 2007;101:570–80.

9. Riemenschneider MJ, Mueller W, Betensky RA, Mohapatra G, Louis DN. *In situ* analysis of integrin and growth factor receptor signaling pathways in human glioblastomas suggests overlapping relationships with focal adhesion kinase activation. Am J Pathol 2005;167:1379–87.

10. Brem RB, Robbins SG, Wilson DJ, et al. Immunolocalization of integrins in the human retina. Invest Ophthalmol Vis Sci 1994;35:3466–74.

11. Oka N, Soeda A, Inagaki A, et al. VEGF promotes tumorigenesis and angiogenesis of human glioblastoma stem cells. Biochem Biophys Res Commun 2007;360: 553–9.

12. Cai W, Wu Y, Chen K, Cao Q, Tice DA, Chen X. *In vitro* and *in vivo* characterization of 64Cu-labeled Abegrin, a humanized monoclonal antibody against integrin $\alpha_v\beta_3$. Cancer Res 2006;66:9673–81.

13. Chatterjee S, Matsumura A, Schradermeier J, Gillespie GY. Human malignant glioma therapy using anti-$\alpha_v\beta_3$ integrin agents. J Neurooncol 2000;46:135–44.

14. Bakewell SJ, Nestor P, Prasad S, et al. Platelet and osteoclast β_3 integrins are critical for bone metastasis. Proc Natl Acad Sci U S A 2003;100:14205–10.

15. Havaki S, Kouloukoussa M, Amawi K, et al. Altered expression pattern of integrin $\alpha_v\beta_3$ correlates with actin cytoskeleton in primary cultures of human breast cancer. Cancer Cell Int 2007;7:16.

16. Hieken TJ, Farolan M, Ronan SG, Shilkaitis A, Wild L, Das Gupta TK. β_3 Integrin expression in melanoma predicts subsequent metastasis. J Surg Res 1996;63: 169–73.

17. Klemke M, Weschenfelder T, Konstandin MH, Samstag Y. High affinity interaction of integrin $\alpha_4\beta_1$ (VLA-4) and vascular cell adhesion molecule 1 (VCAM-1) enhances migration of human melanoma cells across activated endothelial cell layers. J Cell Physiol 2007;212:368–74.

18. Li SG, Ye ZY, Zhao ZS, Tao HQ, Wang YY, Niu CY. Correlation of integrin β_3 mRNA and vascular endothelial growth factor protein expression profiles with the clinicopathological features and prognosis of gastric carcinoma. World J Gastroenterol 2008;14:421–7.

19. Liapis H, Adler LM, Wick MR, Rader JS. Expression of $\alpha_v\beta_3$ integrin is less frequent in ovarian epithelial tumors of low malignant potential in contrast to ovarian carcinomas. Hum Pathol 2007;28:443–9.

20. Sathornsumetee S, Cao Y, Marcello JE, et al. Tumor angiogenic and hypoxic profiles predict radiographic response and survival in malignant astrocytoma patients treated with bevacizumab and irinotecan. J Clin Oncol 2008;26:271–8.

21. Ramos OH, Kauskot A, Cominetti MR, et al. A novel $\alpha_v\beta_3$-blocking disintegrin containing the RGD motive, DisBa-01, inhibits bFGF-induced angiogenesis and melanoma metastasis. Clin Exp Metastasis 2008;25: 53–64.

22. Harris TD, Kalogeropoulos S, Nguyen T, et al. Design, synthesis, and evaluation of radiolabeled integrin $\alpha v\beta 3$ receptor antagonists for tumor imaging and radiotherapy. Cancer Biother Radiopharm 2003;18: 627–41.

23. Fu Y, Ponce ML, Thill M, Yuan P, Wang NS, Csaky KG. Angiogenesis inhibition and choroidal neovascularization suppression by sustained delivery of an integrin antagonist, EMD478761. Invest Ophthalmol Vis Sci 2007;48:5184–90.

24. Yamada S, Bu XY, Khankaldyyan V, Gonzales-Gomez I, McComb JG, Laug WE. Effect of the angiogenesis inhibitor Cilengitide (EMD 121974) on glioblastoma growth in nude mice. Neurosurgery 2006; 59:1304–12.

25. Burke PA, DeNardo SJ, Miers LA, Lamborn KR, Matzku S, DeNardo GL. Cilengitide targeting of $\alpha_v\beta_3$ integrin receptor synergizes with radioimmunotherapy to increase efficacy and apoptosis in breast cancer xenografts. Cancer Res 2002;62:4263–72.

26. Gutheil JC, Campbell TN, Pierce PR, et al. Targeted antiangiogenic therapy for cancer using Vitaxin: a humanized monoclonal antibody to the integrin $\alpha_v\beta_3$. Clin Cancer Res 2000;6:3056–61.

27. Mulgrew K, Kinneer K, Yao XT, et al. Direct targeting of $\alpha_v\beta_3$ integrin on tumor cells with a monoclonal antibody, Abegrin. Mol Cancer Ther 2006;5:3122–9.

28. Grana C, Chinol M, Robertson C, et al. Pretargeted adjuvant radioimmunotherapy with yttrium-90-biotin in malignant glioma patients: a pilot study. Br J Cancer 2002;86:207–12.

29. Julow J, Backlund EO, Lanyi F, et al. Long-term results and late complications after intracavitary yttrium-90 colloid irradiation of recurrent cystic craniopharyngiomas. Neurosurgery 2007;61:288–95.

30. Zinzani PL, Tani M, Fanti S, et al. A phase 2 trial of fludarabine and mitoxantrone chemotherapy followed by yttrium-90 ibritumomab tiuxetan for patients with previously untreated, indolent, nonfollicular, non-Hodgkin lymphoma. Cancer 2008;112:856–62.

31. Iwamoto FM, Schwartz J, Pandit-Taskar N, et al. Study of radiolabeled indium-111 and yttrium-90 ibritumomab tiuxetan in primary central nervous system lymphoma. Cancer 2007;110:2528–34.

32. Pitini V, Baldari S, Altavilla G, Arrigo C, Naro C, Perniciaro F. Salvage therapy for primary central nervous system lymphoma with 90Y-Ibritumomab and Temozolomide. J Neurooncol 2007;3:291–3.

33. Kuzel TM, Rosen ST. Radioimmunotherapy of lymphoma. Cancer Treat Res 1993;68:1–12.

34. Wagner HN, Jr., Wiseman GA, Marcus CS, et al. Administration guidelines for radioimmunotherapy of non-Hodgkin's lymphoma with 90Y-labeled anti-CD20 monoclonal antibody. J Nucl Med 2002;43: 267–72.

35. Martensson L, Wang Z, Nilsson R, et al. Determining maximal tolerable dose of the monoclonal antibody BR96 labeled with 90Y or 177Lu in rats: establishment of a syngeneic tumor model to evaluate means to improve radioimmunotherapy. Clin Cancer Res 2005;11: 7104–8s.

36. Chen X, Park R, Khankaldyyan V, et al. Longitudinal microPET imaging of brain tumor growth with F-18-labeled RGD peptide. Mol Imaging Biol 2006;8:9–15.

37. Chen X, Sievers E, Hou Y, et al. Integrin $\alpha_v\beta_3$-targeted imaging of lung cancer. Neoplasia 2005;7: 271–9.

38. Li ZB, Wu Z, Chen K, Chin FT, Chen X. Click chemistry for ^{18}F-labeling of RGD peptides and microPET imaging of tumor integrin $\alpha_v\beta_3$ expression. Bioconjug Chem 2007;18:1987–94.

39. Krishnan A, Nademanee A, Fung HC, et al. Phase II trial of a transplantation regimen of yttrium-90 ibritumomab tiuxetan and high-dose chemotherapy in patients with non-Hodgkin's lymphoma. J Clin Oncol 2008;26:90–5.

40. Neff R, Abdel-Misih R, Khatri J, et al. The toxicity of liver directed yttrium-90 microspheres in primary and metastatic liver tumors. Cancer Invest 2008;26: 173–7.

41. Zinzani PL, Tani M, Fanti S, et al. A phase II trial of CHOP chemotherapy followed by yttrium-90 ibritumomab tiuxetan (Zevalin) for previously untreated elderly diffuse large B-cell lymphoma patients. Ann Oncol. Epub ahead of print 2008 Feb 25.

42. Goldenberg DM, Griffiths GL. Radioimmunotherapy of cancer: arming the missiles. J Nucl Med 1992;33: 1110–2.

43. Onthank DC, Liu S, Silva PJ, et al. ^{90}Y and ^{111}In complexes of a DOTA-conjugated integrin $\alpha_v\beta_3$ receptor antagonist: different but biologically equivalent. Bioconjug Chem 2004;15:235–41.

44. White CA. Radioimmunotherapy in non-Hodgkin's lymphoma: focus on ^{90}Y-ibritumomab tiuxetan (Zevalin). J Exp Ther Oncol 2004;4:305–16.

45. Chen W, Cloughesy T, Kamdar N, et al. Imaging proliferation in brain tumors with ^{18}F-FLT PET: comparison with ^{18}F-FDG. J Nucl Med 2005;46: 945–52.

46. van Waarde A, Cobben DC, Suurmeijer AJ, et al. Selectivity of ^{18}F-FLT and ^{18}F-FDG for differentiating tumor from inflammation in a rodent model. J Nucl Med 2004;45:695–700.

47. Saga T, Kawashima H, Araki N, et al. Evaluation of primary brain tumors with FLT-PET: usefulness and limitations. Clin Nucl Med 2006;31:774–80.

48. O'Donoghue JA, Bardies M, Wheldon TE. Relationships between tumor size and curability for uniformly targeted therapy with β-emitting radionuclides. J Nucl Med 2005;36:1902–9.

49. Brechbiel MW. Targeted α-therapy: past, present, future? Dalton Trans 2007;4918–28.

50. Multani PS, Grossbard ML. Monoclonal antibody-based therapies for hematologic malignancies. J Clin Oncol 1998;16:3691–710.

51. Bartolomei M, Mazzetta C, Handkiewicz-Junak D, et al. Combined treatment of glioblastoma patients with locoregional pre-targeted ^{90}Y-biotin radioimmunotherapy and temozolomide. Q J Nucl Med Mol Imaging 2004;48:220–8.

52. Boiardi A, Bartolomei M, Silvani A, et al. Intratumoral delivery of mitoxantrone in association with ^{90}Y radioimmunotherapy (RIT) in recurrent glioblastoma. J Neurooncol 2005;2:125–31.

53. Paganelli G, Grana C, Chinol M, et al. Antibody-guided three-step therapy for high grade glioma with yttrium-90 biotin. Eur J Nucl Med 1999;26: 348–57.

54. Williams JA, Edwards JA, Wessels BW, et al. Targeting and therapy of human glioma xenografts *in vivo* using radiolabeled antibodies. Int J Radiat Oncol Biol Phys 1990;19:633–42.

55. Bello L, Lucini V, Giussani C, et al. IS20I, a specific $\alpha_v\beta_3$ integrin inhibitor, reduces glioma growth *in vivo*. Neurosurgery 2003;52:177–85.

56. Taga T, Suzuki A, Gonzalez-Gomez I, et al. α_v-Integrin antagonist EMD 121974 induces apoptosis in brain tumor cells growing on vitronectin and tenascin. Int J Cancer 2002;98:690–7.

Clinical Cancer Research

Integrin $\alpha_v\beta_3$-Targeted Radioimmunotherapy of Glioblastoma Multiforme

Anand Veeravagu, Zhaofei Liu, Gang Niu, et al.

Clin Cancer Res 2008;14:7330-7339.